

Magnus integrators on multicore CPUs and GPUs

N. Auer, L. Einkemmer, P. Kandolf, and A. Ostermann
Department of Mathematics, University of Innsbruck, Austria

December 14, 2024

Abstract

In the present paper we consider numerical methods to solve the Schrödinger equation with a time dependent Hamiltonian. We will consider both short-range interactions, which lead to evolution equations involving sparse matrices, and long-range interactions, which lead to dense matrices. Both of these settings show very different computational characteristics. We use Magnus integrators for time integration and employ a framework based on Leja interpolation to compute the resulting action of the matrix exponential. We consider both traditional Magnus integrators (which are extensively used for these types of problems in the literature) as well as the recently developed commutator-free Magnus integrators and implement them on modern CPU and GPU (graphics processing unit) based systems.

We find that GPUs can yield a significant speed-up (up to a factor of 10 in the dense case) for these types of problems. In the sparse case GPUs are only advantageous for large problem sizes and the achieved speed-ups are more modest. In most cases the commutator-free variant is superior but especially on the GPU this advantage is rather small. In fact, none of the advantage of commutator-free methods on GPUs (and on multi-core CPUs) is due to the elimination of commutators. This has important consequences for the design of more efficient numerical methods.

1 Introduction

To numerically solve the Schrödinger equation with a time-dependent Hamiltonian

$$i \frac{d\psi}{dt} = H(t)\psi(t), \quad \psi(0) = \psi_0, \quad (1)$$

is a problem of significant interest in various fields of quantum mechanics. Applications range from discrete spin systems to (continuous) models of atom-laser interaction. Therefore, it is important to have both, good numerical algorithms, as well as an efficient implementation on state of the art computer hardware of these algorithms at one's disposal.

Magnus integrators are used in many such applications (see, for example, [9, 20, 22, 23, 25]). The implementation of these Magnus integrators (which constitute a subclass of exponential integrators; for more details see [9, 17, 21]) requires the computation of the action of matrix exponentials in an efficient and stable manner. A number of approaches have been proposed in the literature (see, for example, [4, 10, 14, 18, 19, 21]). Most of them are based on polynomial interpolation. In [10, 11] it was shown that interpolation at Leja points is a very efficient way of performing this approximation for the Schrödinger equation. This algorithm interpolates the exponential function and thus reduces the task of computing the action of a matrix exponential to the task of computing a sequence of matrix-vector products. Let us also note that, in addition to the Schrödinger equation considered in this paper, Magnus integrators have been successfully applied to many related problems.

In addition to the matrix exponential, traditional Magnus integrators of higher order require the computation of matrix commutators (see, for example, [8, 9, 21]). In time dependent problems (as those considered here) these matrix commutators have to be computed once every time step. Thus, especially for large problem sizes the corresponding cost can outweigh the cost of the matrix-vector products. Recently, commutator-free Magnus integrators have been developed [5, 7]. They eliminate commutators but usually require additional matrix-vector products.

Due to the trend towards CPUs with more and more cores as well as the trend towards GPUs, providing an efficient implementation of numerical algorithms on modern multi-core CPUs and GPUs is of great practical importance. Some preliminary work on implementing exponential integrators [13] and matrix functions [14] has been conducted on GPUs (with generally promising results). The purpose of the present work is to investigate the performance of both commutator-free and traditional Magnus integrators. This is done in the context of multi-core CPUs and GPUs. Although from

a computational complexity point of view, one might conjecture that computing the commutators will dominate the total computational cost, this is not necessarily true in an actual implementation. In particular, on GPUs matrix-matrix products (necessary for computing the commutators) can operate close to peak efficiency while this is usually not the case for matrix-vector products. The comparison will be performed in the context of both short-range interactions (which lead to sparse Hamiltonians $H(t)$) and long-range interactions (which lead to dense Hamiltonians $H(t)$) to ascertain in which situations GPUs result in a significant gain in performance.

This paper is based, in part, on the thesis [6] and is structured as follows. In section 2 we provide an introduction to Magnus integrators and specify the numerical methods used in the subsequent sections. Section 3 then details the numerical approximation and the implementation. The numerical results are presented and discussed in section 4. Finally, we conclude in section 5.

2 Magnus integrators

The solution of the linear differential equation

$$Y'(t) = A(t)Y(t), \quad Y(0) = Y_0, \quad (2)$$

can be expressed as

$$Y(t) = \exp(\Omega(t))Y_0, \quad (3)$$

where the difficulty lies in finding a suitable matrix $\Omega(t)$. In [24] Magnus used the ansatz of differentiating (3) to find an expression for $\Omega(t)$. This results in

$$Y'(t) = \frac{d}{dt} \exp(\Omega(t))Y_0 = \text{dexp}_{\Omega(t)}(\Omega'(t)) \exp(\Omega(t))Y_0, \quad (4)$$

where the operator dexp is defined as

$$\text{dexp}_{\Omega}(C) = \sum_{k=0}^{\infty} \frac{1}{(k+1)!} \text{ad}_{\Omega}^k(C) = \varphi_1(\text{ad}_{\Omega})(C), \quad (5)$$

see [17]. Here the operator $\text{ad}_{\Omega}^k(C)$ is the iterated commutator and recursively defined as

$$\text{ad}_{\Omega}^j(C) = [\Omega, \text{ad}_{\Omega}^{j-1}(C)], \quad j \geq 1,$$

and $\text{ad}_\Omega^0(C) = C$. Comparing (2) and (4) leads to

$$A(t) = \text{dexp}_{\Omega(t)}(\Omega'(t)), \quad \Omega(0) = 0. \quad (6)$$

By applying the inverse of the derivative of the matrix exponential we obtain a differential equation for Ω . In fact, when $\|\Omega(t)\| < \pi$ the operator $\text{dexp}_{\Omega(t)}$ is invertible and has the convergent series representation

$$\text{dexp}_{\Omega(t)}^{-1}(A(t)) = \sum_{k=0}^{\infty} \frac{\beta_k}{k!} \text{ad}_{\Omega(t)}^k(A(t)),$$

where β_k denote the Bernoulli numbers. As a result we obtain an explicit differential equation for $\Omega(t)$ as

$$\begin{aligned} \Omega'(t) &= \text{dexp}_{\Omega(t)}^{-1}(A(t)) \\ &= A(t) - \frac{1}{2} [\Omega(t), A(t)] + \frac{1}{12} [\Omega(t), [\Omega(t), A(t)]] + \dots . \end{aligned} \quad (7)$$

Equation (7) can be integrated by Picard iteration and this leads to the so-called *Magnus expansion*,

$$\begin{aligned} \Omega(t) &= \int_0^t A(t_1) dt_1 - \frac{1}{2} \int_0^t \left[\int_0^{t_1} A(t_2) dt_2, A(t_1) \right] dt_1 \\ &\quad + \frac{1}{4} \int_0^t \left[\int_0^{t_1} \left[\int_0^{t_2} A(t_3) dt_3, A(t_2) \right] dt_2, A(t_1) \right] dt_1 \\ &\quad + \frac{1}{12} \int_0^t \left[\int_0^{t_1} A(t_2) dt_2, \left[\int_0^{t_1} A(t_2) dt_2, A(t_1) \right] \right] dt_1 + \dots . \end{aligned} \quad (8)$$

To derive numerical methods from the Magnus expansion we assume a constant time step size τ and thus the solution after one time step is

$$Y(t_n + \tau) = \exp(\Omega(t_n + \tau))Y(t_n), \quad (9)$$

resulting in the numerical scheme

$$Y_{n+1} = \exp(\Omega_n)Y_n, \quad (10)$$

for a suitable approximation Ω_n of $\Omega(t_n + \tau)$. One way of deriving a formula for Ω_n is to approximate the integrals in (8) by quadrature rules.

In the following we will introduce the three traditional Magnus integrators that are used for the numerical experiments in Section 4.

Method 1 (M2). The first example is the simplest method, which is obtained by truncating the series (8) after the first term and approximating the integral by the midpoint rule. This yields

$$\Omega_n(\tau) = \tau A \left(t_n + \frac{\tau}{2} \right)$$

as an approximation of $\Omega(t_n + \tau)$. The corresponding numerical scheme is the exponential midpoint rule

$$Y_{n+1} = \exp \left(\tau A \left(t_n + \frac{\tau}{2} \right) \right) Y_n,$$

which is of order two.

Method 2 (M4). The second example is a scheme of order four. The Magnus series (8) is truncated after the second term and the integrals are approximated by the two-stage Gauss quadrature rule with weights $b_1 = b_2 = \frac{1}{2}$ and nodes $c_1 = \frac{1}{2} - \frac{\sqrt{3}}{6}$, $c_2 = \frac{1}{2} + \frac{\sqrt{3}}{6}$. We obtain

$$Y_{n+1} = \exp \left(\frac{\tau}{2} (A_1 + A_2) + \frac{\sqrt{3}\tau^2}{12} [A_2, A_1] \right) Y_n,$$

where $A_1 = A(t_n + c_1\tau)$ and $A_2 = A(t_n + c_2\tau)$.

Method 3 (M6). As a third example, we consider the following scheme of order six:

$$Y_{n+1} = \exp \left(B_1 + \frac{1}{2} B_3 + \frac{1}{240} \left[-20B_1 - B_3 + [B_1, B_2], B_2 - \frac{1}{60} [B_1, 2B_3 + [B_1, B_2]] \right] \right) Y_n,$$

where A_i is an approximation of $A(t_n + c_i\tau)$ for

$$c_1 = \frac{1}{2} - \frac{\sqrt{15}}{10}, \quad c_2 = \frac{1}{2}, \quad c_3 = \frac{1}{2} + \frac{\sqrt{15}}{10},$$

and

$$B_1 = \tau A_2, \quad B_2 = \frac{\sqrt{15}}{3} \tau (A_3 - A_1), \quad B_3 = \frac{10}{3} \tau (A_3 - 2A_2 + A_1).$$

As has been discussed in the introduction, the (nested) commutators arising in methods 2 and 3 can be expensive to compute. Thus, in addition, we consider commutator free Magnus methods (see [7]). To achieve this our aim is to find an approximation of the form

$$Y(t_n + \tau) \approx Y_{n+1} = \exp\left(\Omega_n^{(1)}\right) \exp\left(\Omega_n^{(2)}\right) \cdots \exp\left(\Omega_n^{(s)}\right) Y_n,$$

with

$$\Omega_n^{(i)} = \tau \sum_{j=1}^J \alpha_{ij} A_j, \quad \text{for } i = 1, \dots, s.$$

Here $A_i = A(t_n + c_i \tau)$ again denotes the evaluation of the matrix A at a certain time. More precisely, the goal is to find $\Omega_n^{(1)}, \dots, \Omega_n^{(s)}$ such that

$$\exp\left(\Omega_n^{(1)}\right) \exp\left(\Omega_n^{(2)}\right) \cdots \exp\left(\Omega_n^{(s)}\right) = \exp(\Omega_n) + \mathcal{O}(\tau^{s+1})$$

by determining s , J and α_{ij} for $i = 1, \dots, s$ and $j = 1, \dots, J$. The matrix $\Omega_n \approx \Omega(t_n + \tau)$ is the matrix at time step n of an S th order Magnus method given as in (10). In the numerical experiments we will use the following numerical method that has been derived in [7].

Method 4 (Cf4). For $c_1 = \frac{1}{2} - \frac{\sqrt{3}}{6}$, $c_2 = \frac{1}{2} + \frac{\sqrt{3}}{6}$, as well as $\alpha_1 = \frac{3-2\sqrt{3}}{12}$, and $\alpha_2 = \frac{3+2\sqrt{3}}{12}$ a commutator-free method of order 4 is given by

$$\begin{aligned} Y_{n+1} &= \exp\left(\Omega_n^{(1)}\right) \exp\left(\Omega_n^{(2)}\right) Y_n \\ &= \exp\left(\tau(\alpha_1 A_1 + \alpha_2 A_2)\right) \exp\left(\tau(\alpha_2 A_1 + \alpha_1 A_2)\right) Y_n. \end{aligned}$$

In Figure 1 we show the error as a function of the time step size. This, serves to check the order of the four methods discussed in this section and helps in validating our implementation. We also note that the Cf4 method requires two matrix exponentials but no commutator and is somewhat more accurate compared to the M4 method (which requires only a single matrix exponential but the computation of one-commutator).

3 Numerical approximation and implementation

So far we have not discussed how to approximate the action of the matrix exponential. That is, how to compute

$$Y_{n+1} = \exp(\Omega_n) Y_n.$$

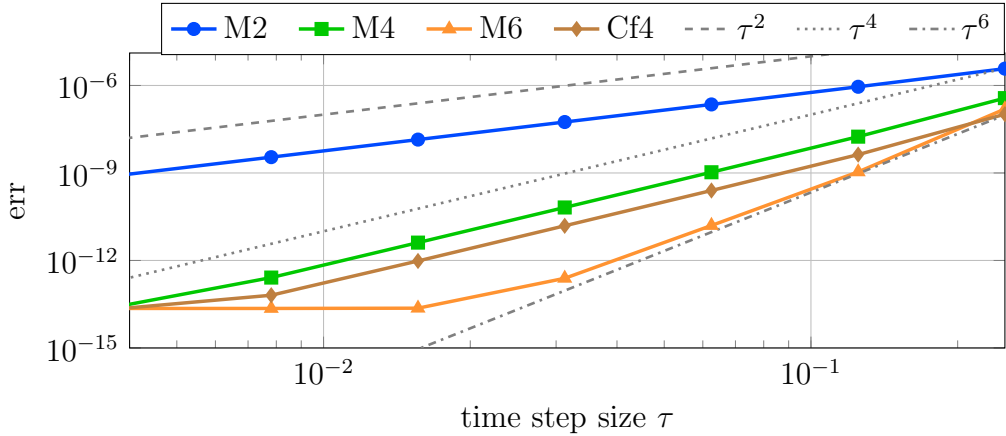


Figure 1: Order plot for the methods M2 (blue with dots), M4 (green with squares), M6 (orange with triangles), and Cf4 (brown with diamonds). For Example 1 with $N = 2^{10}$ and varying time step size τ .

It is not viable to compute $\exp(\Omega_n)$ and then apply it to the vector Y_n . Furthermore, if Ω_n is sparse, this is, in general, not the case for $\exp(\Omega_n)$ and thus a significant penalty in terms of memory is implied. However, a number of approaches to efficiently compute the action of a matrix exponential have been developed in the literature. Probably the most prominent are Krylov subspace methods, interpolation at Chebyshev points, the truncated Taylor method, and interpolation at Leja points. For all of these methods the main cost to approximate Y_{n+1} are matrix-vector products.

In the numerical results presented in the next section we will exclusively use interpolation at Leja point (the method described in [11]). This method is favorably compared to interpolation at Chebyshev points as the order of the interpolation polynomial can be chosen adaptively. In addition, it has been shown in [10] that interpolation at Leja points can be superior to using Krylov methods. In addition, in contrast to Krylov subspace methods, only few vectors have to be kept in memory. This reduces the memory footprint of the Leja interpolation which is especially helpful for the GPU implementation, where memory is a more scarce resource compared to traditional CPU systems.

The main idea of the Leja method is to approximate the exponential by an interpolation polynomial. The interpolation nodes ξ_0, \dots, ξ_m for a polynomial of degree m are chosen to be Leja points (see [11], for a precise definition). The corresponding interpolation polynomial is expressed in Newton form and therefore the main cost of the algorithm is contained in a short term recurrence formula that performs matrix-vector products.

Let $p_m(A)v$ be the interpolation polynomial of degree m that approximates the action of the exponential of the matrix A applied to the vector v . Furthermore, we denote by $d_i := \exp[\xi_0, \xi_1, \dots, \xi_i]$ the divided differences of order i . Then Leja interpolation has the form

$$\exp(A)v \approx p_m(A)v = \sum_{i=0}^m d_i \prod_{j=0}^{i-1} (A - \xi_j I)v,$$

and can be implemented by the following code fragment

```

1  w = v
2  p = d0v
3  for i = 1 : m
4      w = Aw - xi-1w
5      p = p + diw

```

The actual implementation is more involved. It makes sure that the backward error of the interpolation is below a user specified tolerance (up to the unit round-off). Furthermore, an early termination criterion is implemented to reduce the cost further. For more details we refer the reader to [11].

It should be noted that the Leja method is not entirely matrix-free. In fact the matrix itself is required for estimating the necessary parameters of the interpolation (i.e. an estimate on the spectrum of the matrix). Nevertheless, we can think of these parameters as fixed and therefore the performance of the method breaks down to performing the above code fragment as fast as possible.

The speed of the numerical method is highly dependent on the underlying implementation of matrix-vector products (to compute the Leja interpolation) and matrix-matrix products (to compute the commutators). The Leja interpolation routines are implemented as part of the *expleja* project¹ in a generic fashion. That is, for all of the implementations the core Leja algorithm is the same. We use the preprocessor to switch out the calls to the matrix-vector and matrix-matrix product routines. Thus, the library is designed in such a way that it is easy to include your favorite library dealing with matrices, vectors, and most importantly the matrix-vector and matrix-matrix products.

In this paper we are concerned with traditional CPUs and GPUs as well as dense and sparse matrices. In the numerical experiments in the next section, we use the standard BLAS² and Intel Math Kernel Library (MKL)³ [1]

¹see <https://bitbucket.org/expleja/expleja>

²Version: gcc 4.8.4, libblas-dev: 1.2.20110419-7

³Version: icc 15.0.0 20140723, MKL 2017.0.098

routines for dense matrices on the CPU, SuiteSparse⁴ [12] and Intel MKL for spare matrices on the CPU, and the CUDA libraries cuBLAS and cuSPARSE⁵ [2, 3] for dense and sparse matrices, respectively, on the GPU.

The probably most widely used sparse matrix storage scheme is the compressed sparse row (CSR) format (see, for example, [3]). This format can store arbitrary sparse matrices and is extensively used in a range of applications. In addition, the CSR format enjoys universal support from almost all sparse matrix libraries. It should be noted, however, that specific sparse matrix formats have been developed that allow for a more favorable memory access pattern and consequently improved performance on GPUs. However, as recent research [15, 16, 26] shows the potential improvement compared to a well implemented CSR algorithm is at best 60 %. In addition, the magnitude of improvement is highly problem dependent. Due to this and due to ubiquity of the CSR format we will make exclusive use of it in the present paper.

To allow a fair comparison and to enable other scientists to take advantage of our implementation the code is available via the *expleja* project.

Let us further note that in the case of the GPU implementation we make sure that we move data from the CPU to the GPU (or in the other direction) only if necessary. More specifically, we transfer all input data at the beginning of the computation, perform all the numerical computation on the GPU, and finally only the output data is transferred back to the CPU. Consequently, in all instances the data transfer from and to the GPU takes only a negligible amount of time.

The following hardware is used in all of the experiments

CPU	GPU
• 2 × Intel Xeon E5-2630 CPU	• Tesla K80
• 2 × 8 cores	• 4992 CUDA Cores
• 32GB Ram	• 2 × 12 GB RAM

Before proceeding, it is instructive to discuss the performance characteristics of the two main ingredients in the Magnus integrator. Namely, the matrix-vector products required for the Leja interpolation and the matrix-matrix products required for assembling the matrix (the latter are only required for the Magnus integrators that involve commutators). Since the matrix is time dependent we have to assemble the matrix (and thus compute

⁴Version: gcc 4.8.4, libsuitesparse-dev: 1:4.2.1-3ubuntu1

⁵Version: nvcc 7.0.27, CUDA Toolkit 7.5

the commutators) in every time step. A straightforward complexity analysis leads us to conclude that the matrix-matrix products dominate the run time of the algorithm. In fact, this is consistent with what we will observe in the next section for the sequential version of the code. Since for traditional higher order Magnus integrators the number of required commutators can be quite large, research has been conducted in both reducing [8] and completely eliminating (commutator-free approach) [7] commutators from the numerical method.

However, this analysis is too simplistic to accurately reflect the performance of the numerical method in an actual implementation. The first point to make here is that potentially a large number of matrix-vector products are needed in each time step. This is in particular true for matrices with large eigenvalues in the left half of the complex plane (i.e. for stiff problems). This behavior alone is sufficient to make a purely theoretical analysis difficult. However, there is a second aspect that needs to be taken into account on modern computer hardware (both on multi-core CPUs and on GPUs). Namely, that the matrix-matrix products constitute a compute bound problem and thus can be parallelized very efficiently, while matrix-vector products are memory bound and are thus limited by the (much slower) memory bandwidth.

To be more specific let us consider the dense case. We have implemented a test case for both the matrix-vector as well as matrix-matrix products. The parallel implementation using Intel MKL on the CPU saturates with only 4 cores (although 16 are available on above mentioned system; a behavior that is characteristic for memory bound problems) achieving approximately 10 GFlop/s. This constitutes approximately 70 % of the theoretical memory bandwidth but only a small fraction of the GFlop/s that are available on that system. On the other hand, the parallel implementation of the matrix-matrix products using Intel MKL yields approximately 150 GFlop/s. Thus, while the computational complexity of the matrix-matrix products is far worse, in a parallel setting, the constants are potentially much smaller. To conclude this section let us note that essentially the same behavior occurs on the GPU and that we will revisit this issue again in the next section when we discuss the numerical results.

4 Numerical experiments

In the following discussion “host” refers to the CPU and “device” refers to the GPU. For the Intel MKL implementation on the CPU we tested various number of threads and used the configuration that gives the best perfor-

mance. The time of the computation is measured by taking the difference of calling `clock()` before and after the time integration. The result is converted to seconds. For all of the experiments we compute a reference solution on the GPU with the method M6 and a fixed time step size of $\tau = 10^{-5}$. If not specified explicitly, the Leja method is used with a relative and absolute tolerance of 10^{-10} and the early termination criterion is activated.

In order to illustrate the behavior of the considered Magnus integrators and their corresponding implementation we consider the Schrödinger equation

$$i\partial_t\psi(t) = H(t)\psi(t), \quad \psi(0) = \psi_0.$$

More specifically, we consider a Heisenberg model. This model is often used in quantum mechanics to describe the spins of a magnetic system. A spin describes a magnetic dipole, where the direction of the spin corresponds to the magnetic moment.

We investigate the performance for both sparse and dense matrices $H(t)$. Physically, this corresponds to a short-range (sparse) and long-range (dense) interaction. We will refer to these situations as the local and non-local model, respectively. As each spin is described by a two dimensional (complex) vector the resulting Hamiltonian $H(t)$ is described by a $2^n \times 2^n$ complex matrix, where n corresponds to the amount of spins in the model. In the following, we use the notation $N = 2^n$.

We discuss the particular shape of the two models used in the corresponding examples. Both rely on the three Pauli matrices

$$\sigma^x = \begin{pmatrix} 0 & 1 \\ 1 & 0 \end{pmatrix}, \quad \sigma^y = \begin{pmatrix} 0 & -i \\ i & 0 \end{pmatrix} \quad \text{and} \quad \sigma^z = \begin{pmatrix} 1 & 0 \\ 0 & -1 \end{pmatrix}. \quad (11)$$

Furthermore we define

$$\sigma_j^\alpha = (\otimes_{i=1}^{j-1} I) \otimes \sigma^\alpha \otimes (\otimes_{i=j+1}^n I), \quad (12)$$

for $\alpha \in \{x, y, z\}$, where \otimes denotes the tensor product. As initial value $\psi_0 \in \mathbb{C}^{2^n}$, we use

$$\psi_0 = (1 \ 0, \ 0 \ 1, \ \psi_0^5 \ \psi_0^6, \ \psi_0^7 \ \dots)^T, \quad (13)$$

where the entries ψ_0^5 to ψ_0^N are chosen randomly such that $\|(\psi_0^i \ \psi_0^{i+1})\|_2 = 1$ for i odd. The initial value is chosen such that the spins 1 and 2 are in a defined state (up and down, respectively). Due to the coupling with the other spins these two spins will leave this pure state and move into a neutral position. This behavior can be observed in the numerical experiments.

In all of our experiments we split up the matrix $H(t)$ as $H(t) = H_1 + h(t)H_2$ where the matrices H_1 and H_2 are computed before the actual time integration on either the host or the device. In particular this means the matrix $H(t)$ is formed on the device without transferring any data from the host. Furthermore, the commutators required for the various tested Magnus integrators are computed directly on the device as well.

Example 1 (Dense matrix case). For the dense case, we use a non-local Heisenberg model, where all spins are coupled. This results in a dense matrix. With the help of the Pauli matrices and σ_j^α , see (11) and (12), we state the non-local Heisenberg model

$$H(t) = - \sum_{i=1}^n \sum_{\substack{j=1 \\ j \neq i}}^n J_{ij} \sigma_i^z \sigma_j^z - \sum_{i=1}^n h(t) \sigma_i^x \in \mathbb{C}^{2^n \times 2^n},$$

where $J_{ij} = \frac{1}{|i-j|}$, $h(t) = \sin(\omega t)$. The initial value $\psi_0 \in \mathbb{C}^{2^n}$ is given by (13). We note that the matrix $H(t)$ consists of two time independent parts that are coupled by $h(t)$. In particular we have $H(t) = H_1 + h(t)H_2$, for

$$H_1 = - \sum_{i=1}^n \sum_{\substack{j=1 \\ j \neq i}}^n J_{ij} \sigma_i^z \sigma_j^z \quad \text{and} \quad H_2 = - \sum_{i=1}^n \sigma_i^x.$$

We exploit this structure in our implementation by assembling the matrices H_1 and H_2 before the actual time integration. This allows us to considerably reduce the computational cost.

In the experiments illustrated in Figures 2 and 3 we fix the time step size to $\tau = 10^{-3}$ and vary the size of the matrices from $N = 2^6$ to $N = 2^{13}$.

In the first experiment we take a look how the parallelization influences the method. In Figure 2 we can observe that for large enough matrices all methods benefit from GPU acceleration, compared to the single-core CPU implementation. Where exactly this benefit kicks in depends on the method. The speed-up is most significant for the methods M4 and M6 that need the computation of matrix commutators. In this case we can achieve a speed-up of nearly one hundred compared to the single-core implementation. The same is true for the parallelization on CPUs where the speed advantage is already significant for small problems. With regard to the methods without commutators (M2 and Cf4) we only observe a maximal speed-up on the GPU of about 10, compared to the single core implementation. It should be noted, however, that in this case the parallelization on the CPUs does not result in as much gain in performance (compared to M4 and M6).

In Figure 3 we show how the four different methods compare on the same hardware. If we first focus on the single core implementation (top) we can see that M2 has the least computational cost. In fact the cost grows as $\mathcal{O}(N^2)$ which roughly corresponds to the cost of the matrix-vector products in the Leja interpolation. This is also the case for the Cf4 method, where no commutator is required but two matrix exponentials have to be computed. As a result the method needs more time per time step compared to M2 but has about the same growth rate. The methods M4 and M6 grow with order three, corresponding to the cost of the matrix-matrix products arising in the commutators.

By using 4 CPUs (middle) we can see that the cost of the methods move together. M2 and M4 need about the same, M6 slightly more and Cf4 turns out to be the most expensive method (per time step). In general, we observe a growth rate of about $\mathcal{O}(N^2)$ for all methods as the matrix-matrix products can be parallelized very efficiently.

If we move to the GPU (bottom) we observe that the growth for all methods is linear until about 2^{10} where full capacity of the GPU is reached. After this we observe that the different methods start to behave similar as for the single CPU, but they are much faster.

In our final experiment we change the setup. This time we fix the matrix size to $N = 2^{12}$, prescribe a certain tolerance, and compare the cost of each method, for each of the parallelization techniques, to achieve the specified tolerance. The matrix size is chosen such that a GPU parallelization makes sense. We note that in all cases the Leja method with the prescribed tolerance divided by 10 is used (that is, a more accurate approximation is used for the polynomial interpolation compared to the time integrator). The results can be found in Figure 4. In the plot the line style corresponds to the methods, full for M2, dashed for M4, dotted for M6, and dash-dotted for Cf4. The marker shape (and the color) correspond to the different parallelization. A (blue) circle for single-core CPU, a (green) square for multi-core CPU, and a (orange) triangle for GPU implementation.

From this plot we can see that the GPU implementation is highly beneficial. For all methods the GPU achieves a speed-up of roughly 10 compared to the multi-core, and about 20 compared to the single-core implementation. Furthermore, we can observe that overall the Cf4 method is the most efficient method in terms of accuracy versus computation time. On the other hand it is clear that for high accuracy the M2 method is not favorable. This is due to the fact that this method is only second order accurate.

For the GPU implementation the methods M4, M6, and Cf4 are very close together, with a cost difference of about 3. For the two CPU implementations this is different. Here Cf4 is clearly the fastest and the difference to M4 and

M6 is approximately a factor of 5 and 10 for the multi- and single-core CPU implementation, respectively.

An important point to make here is that the majority of the computational advantage of the Cf4 method for multi-core CPUs and GPUs is due to its increased accuracy (see Figure 1) and not due to any advantage in cost per time step. In fact, Figure 3 shows that almost all of the advantage in cost (which is clearly significant in the sequential case) is lost once we consider the multi-core CPU or GPU implementation.

Example 2 (Sparse matrix case). For the sparse case we use a local Heisenberg model. Here only neighboring spins are coupled and therefore the corresponding matrix is sparse. With the help of the Pauli matrices, see (11) and (12), we state the local Heisenberg model

$$H(t) = -\frac{1}{2} \sum_{j=1}^n (J_x \sigma_j^x \sigma_{j+1}^x + J_y \sigma_j^y \sigma_{j+1}^y + J_z \sigma_j^z \sigma_{j+1}^z + h(t) \sigma_j^z) \in \mathbb{C}^{2^n \times 2^n},$$

where $J_x, J_y, J_z \in \mathbb{C}$, and $h(t) = \sin(\omega t)$. The initial value is given in (13). For the numerical tests we chose $J_x = 1$, $J_y = 2$, and $J_z = 3$.

Again we note that the matrix $H(t)$ consists of two time independent parts that are coupled by $h(t)$. We split-up the equation in a similar fashion as for the dense model to save computational cost.

In the experiments illustrated by Figures 5, 6, and 7 we fix the time step size to $\tau = 10^{-3}$ and vary the size of the matrices from $N = 2^6$ to $N = 2^{14}$.

In the first experiment, illustrated in Figure 5, we take a look on how the parallelization influences the performance of the methods. Here the GPU implementation does not achieve as high speed-ups as we observed for the dense case. Only for the M6 method we can observe a significant gain for medium sized matrices. In this case we need to compute nested commutators for which the GPU acceleration is highly beneficial. In all other cases the GPU is only favorable once we employ 2^{12} or more degrees of freedom. For small matrices the two CPU implementations are clearly more beneficial.

The second experiment, in Figure 6, compares how the methods perform for each implementation. The M6 method is clearly outperformed by the three other methods, regardless of the implementation. We can see that for the single- and multi-core CPU implementation the growth rate roughly corresponds to the cost of the sparse matrix-matrix products. The GPU has a slightly lower growth rate but not as significant as for the dense case.

As a consistency check, we show that even though the parallelization of the sparse matrices is not as beneficial, compared to the dense case, overall sparse algorithms still pay off significantly. This can be clearly seen in Figure 7. Note, however, that the difference between the two implementations

is significantly smaller for the GPU implementation compared to both CPU implementations. Of course, a further advantage of the sparse algorithms are that they consume less memory and we are thus able to solve larger problems.

Finally, we compare the cost of each method, for each of the parallelization techniques, to achieve a specified tolerance. The matrix size is fixed to $N = 2^{12}$. The results are shown in Figure 8. We observe that in this situation the CPU implementation of the Cf4 method gives the best result overall. It is also interesting to note that the performance of Cf4 and M4 are very similar for the GPU implementation.

5 Conclusion

In this work we have investigated whether parallelization on GPUs is a viable option for Magnus integrators based on Leja interpolation. The numerical solutions have been computed in the context of the Schrödinger equation using a local and a non-local Heisenberg model. Implementing these algorithms on modern multi-core CPU and GPU systems shows that in the dense case the GPU implementation is able to achieve speed-ups of up to a factor of 10. In the sparse case only very large problems benefit from GPU acceleration and the achieved speed-ups are more modest.

From a numerical analysis point of view we observe that the commutator-free fourth order method (Cf4) is usually the best choice. Although for both multi-core CPUs and GPUs the traditional fourth order exponential integrator (M4) is usually quite competitive. This is in stark contrast to the sequential case, where M4 is significantly slower compared to the Cf4 method. This behavior is due to the fact that the matrix-matrix products required to compute the commutators can be more efficiently parallelized. In fact, the per time step cost of the Cf4 is even larger compared to M4. This has important implications for future research in constructing more efficient Magnus type integrators, as modern hardware calls into question the design philosophy of eliminating matrix-matrix products at all costs (at least this is true for the problem sizes currently accessible on a workstation).

References

- [1] Intel MKL Library: documentation. <https://software.intel.com/en-us/intel-mkl/documentation>, 2016. Accessed: 25 October 2016.

- [2] cuBLAS Library: documentation. <http://docs.nvidia.com/cuda/cublas/>, 2016. Accessed: 25 October 2016.
- [3] cuSPARSE Library: documentation. <http://docs.nvidia.com/cuda/cusparse/>, 2016. Accessed: 25 October 2016.
- [4] A.H. Al-Mohy and N.J. Higham. Computing the action of the matrix exponential, with an application to exponential integrators. *SIAM J. Sci. Comput.*, 33(2):488–511, 2011.
- [5] A. Alvermann and H. Fehske. High-order commutator-free exponential time-propagation of driven quantum systems. *J. Comput. Phys.*, 230(15):5930–5956, 2011.
- [6] N. Auer. Magnus integrators on graphics processing units. Master’s thesis, University of Innsbruck, 2016.
- [7] S. Blanes and P.C. Moan. Fourth- and sixth-order commutator-free Magnus integrators for linear and non-linear dynamical systems. *Appl. Numer. Math.*, 56(12):1519–1537, 2006.
- [8] S. Blanes, F. Casas, and J. Ros. Improved high order integrators based on the Magnus expansion. *BIT Numerical Mathematics*, 40(3):434–450, 2000.
- [9] S. Blanes, F. Casas, J. A. Oteo, and J. Ros. The Magnus expansion and some of its applications. *Phys. Rep.*, 470(5–6):151–238, 2009.
- [10] M. Caliari, P. Kandolf, A. Ostermann, and S. Rainer. Comparison of software for computing the action of the matrix exponential. *BIT Numerical Mathematics*, 54(1):113–128, 2014.
- [11] M. Caliari, P. Kandolf, A. Ostermann, and S. Rainer. The Leja method revisited: backward error analysis for the matrix exponential. *SIAM J. Sci. Comput.*, 38(3):A1639–A1661, 2016.
- [12] T.A. Davis. *Direct methods for sparse linear systems*, volume 2 of *Fundamentals of Algorithms*. Society for Industrial and Applied Mathematics (SIAM), Philadelphia, PA, 2006.
- [13] L. Einkemmer and A. Ostermann. Exponential integrators on graphic processing units. In *High Performance Computing and Simulation (HPCS), 2013 International Conference on*, pages 490–496. IEEE, 2013.

- [14] M.E. Farquhar, T.J. Moroney, Q. Yang, and I.W. Turner. GPU accelerated algorithms for computing matrix function vector products with applications to exponential integrators and fractional diffusion. *SIAM J. Sci. Comput.*, 38(3):C127–C149, 2016.
- [15] J.L. Greathouse and M. Daga. Efficient sparse matrix-vector multiplication on GPUs using the CSR storage format. In *Proceedings of the International Conference for High Performance Computing, Networking, Storage and Analysis*, pages 769–780. IEEE Press, 2014.
- [16] D. Guo, W. Gropp, and L.N. Olson. A hybrid format for better performance of sparse matrix-vector multiplication on a GPU. *Int. J. High Perform. Comput. Appl.*, 30(1):103–120, 2016.
- [17] E. Hairer, C. Lubich, and G. Wanner. *Geometric numerical integration. Structure-preserving algorithms for ordinary differential equations*. Springer, Berlin, second edition, 2006.
- [18] N.J. Higham. *Functions of matrices: theory and computation*. SIAM, 2008.
- [19] M. Hochbruck and C. Lubich. On Krylov subspace approximations to the matrix exponential operator. *SIAM J. Numer. Anal.*, 34(5):1911–1925, 1997.
- [20] M. Hochbruck and C. Lubich. On Magnus integrators for time-dependent Schrödinger equations. *SIAM J. Numer. Anal.*, 41(3):945–963, 2003.
- [21] M. Hochbruck and A. Ostermann. Exponential integrators. *Acta Numer.*, 19:209–286, 2010.
- [22] K. Kormann, S. Holmgren, and H.O. Karlsson. Accurate time propagation for the Schrödinger equation with an explicitly time-dependent Hamiltonian. *J. Chem. Phys.*, 128(18):184101, 2008.
- [23] T.V. Laptyeva, E.A. Kozinov, I.B. Meyerov, M.V. Ivanchenko, S.V. Denisov, and P. Hänggi. Calculating Floquet states of large quantum systems: A parallelization strategy and its cluster implementation. *Comput. Phys. Commun.*, 201:85–94, 2016.
- [24] W. Magnus. On the exponential solution of differential equations for a linear operator. *Comm. Pure Appl. Math.*, 7:649–673, 1954.

- [25] H. De Raedt and K. Michielsen. Computational Methods for Simulating Quantum Computers. *Handbook of Theoretical and Computational Nanotechnology* (American Scientific Publishers), 2008.
- [26] J. Zhang, J. Wan, F. Li, J. Mao, L. Zhuang, J. Yuan, E. Liu, and Z. Yu. Efficient sparse matrix–vector multiplication using cache oblivious extension quadtree storage format. *Future Gener. Comput. Syst.*, 54:490–500, 2016.

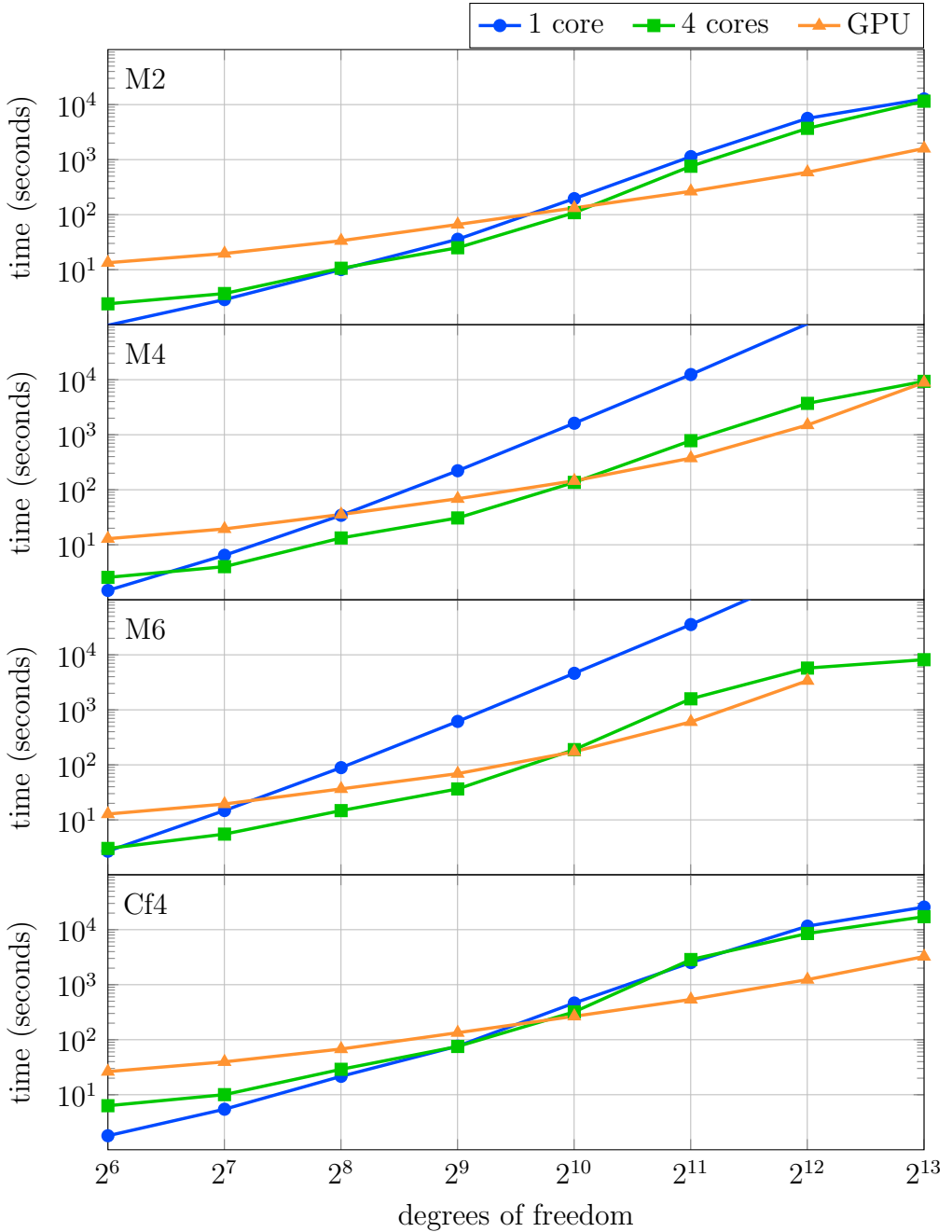


Figure 2: Computational cost vs. degrees of freedom for three different parallelizations of the four integrators M2, M4, M6, and Cf4, grouping by the different methods. The data correspond to Example 1 (dense matrix) with fixed time step size $\tau = 10^{-3}$ for computing $\psi(1)$.

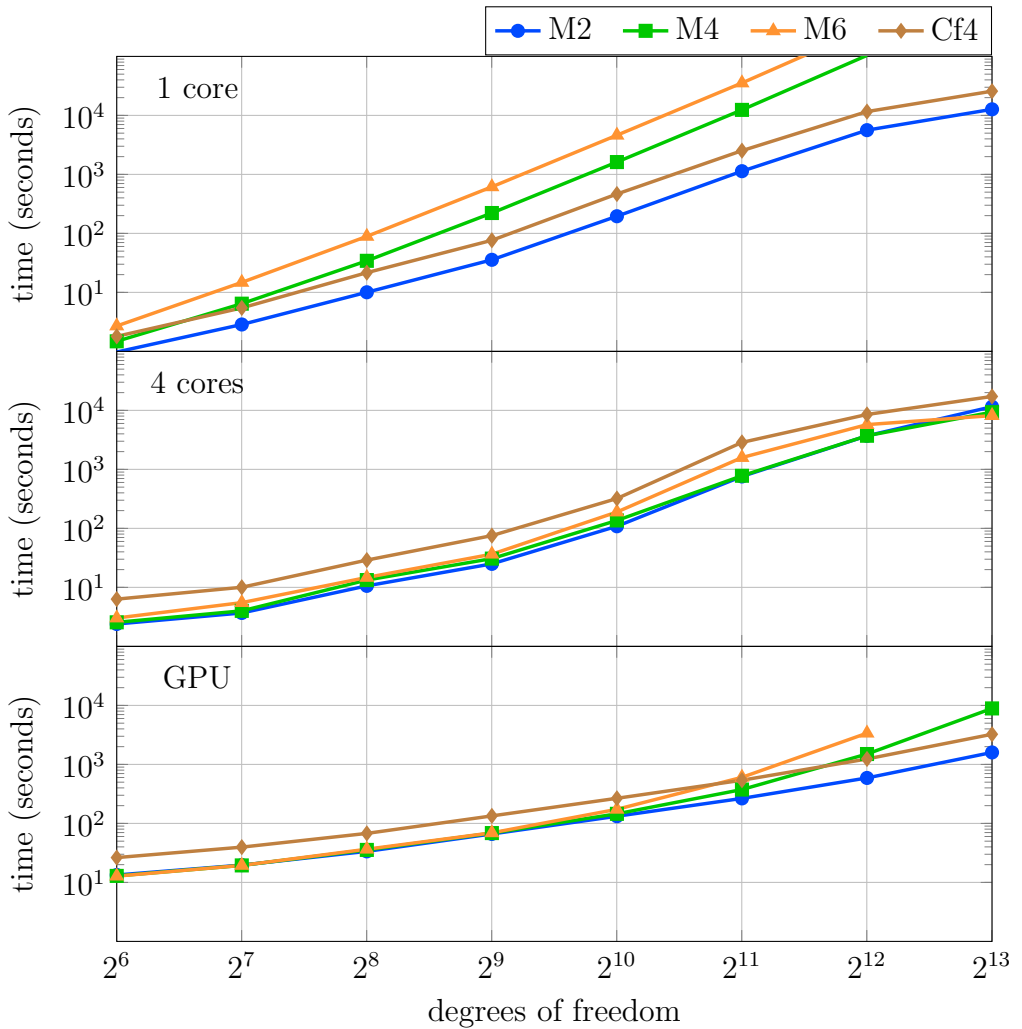


Figure 3: Computational cost vs. degrees of freedom for three different parallelizations of the four integrators M2, M4, M6, and Cf4, grouping by different parallelizations. The data correspond to Example 1 with fixed time step size $\tau = 10^{-3}$ for computing $\psi(1)$.

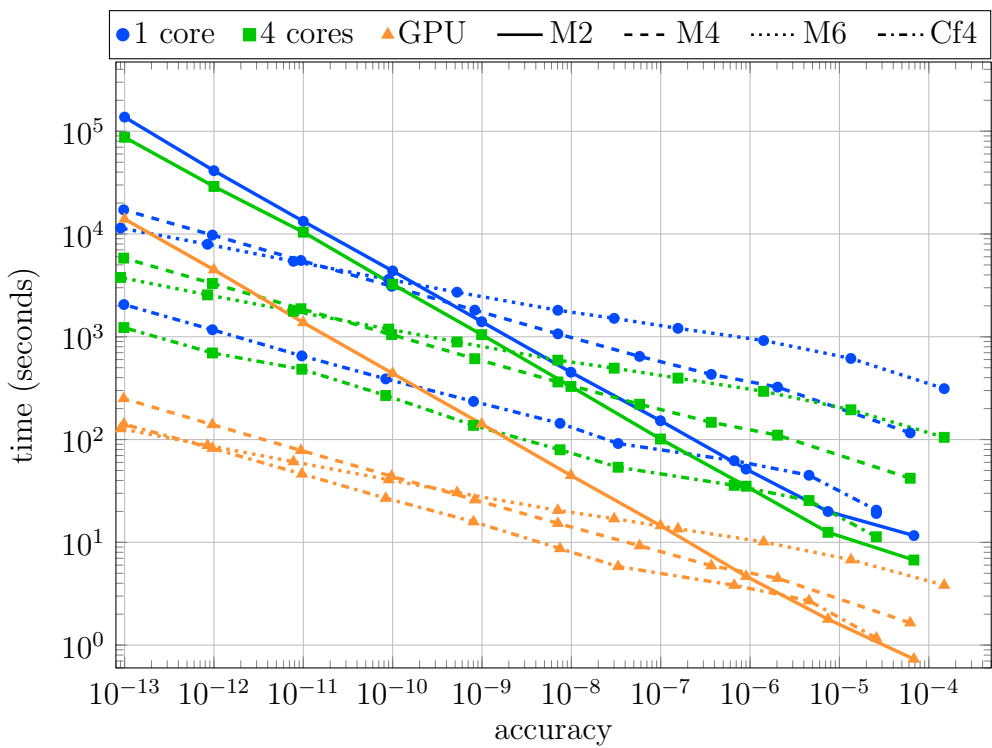


Figure 4: Accuracy vs. computational cost for the four integrators M2, M4, M6, and Cf4 when using different parallelization techniques. The data correspond to Example 1 with fixed matrix dimension $N = 2^{12}$. For a fixed step size τ the error at $\psi(1)$ is measured.

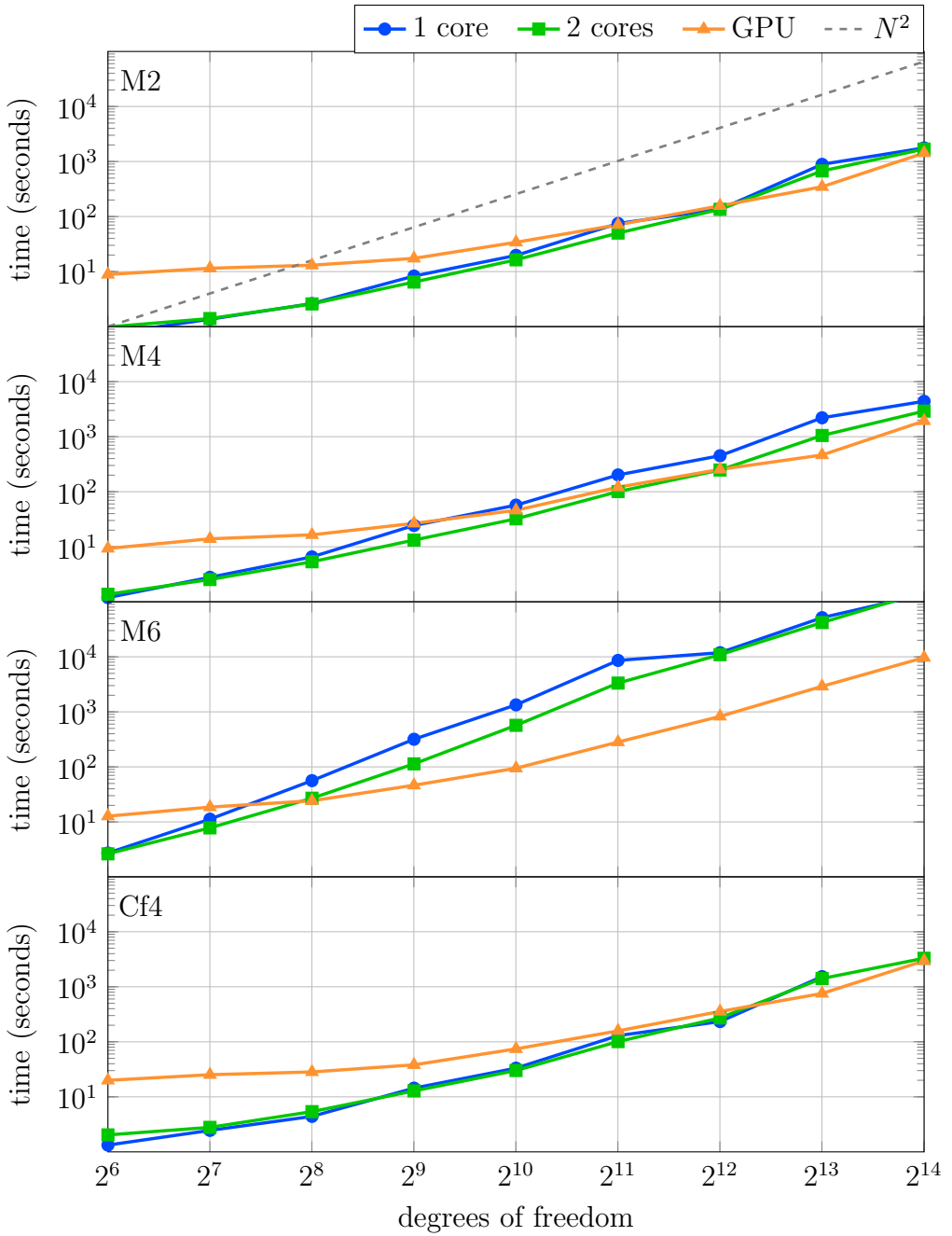


Figure 5: Computational cost vs. degrees of freedom for three different parallelizations of the four integrators M2, M4, M6, and Cf4, grouping different parallelizations. The data correspond to Example 2 with fixed time step size $\tau = 10^{-3}$ for computing $\psi(1)$.

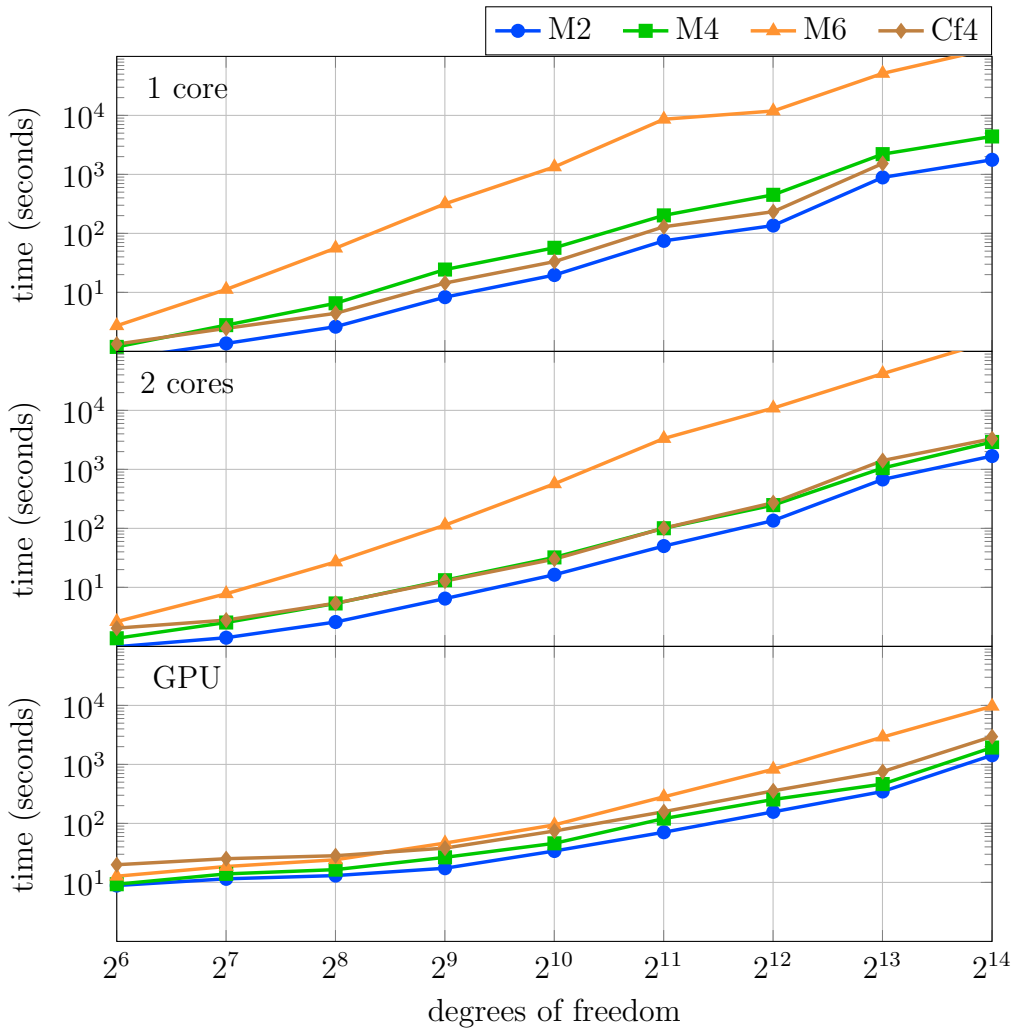


Figure 6: Computational cost vs. degrees of freedom for three different parallelization of the four integrators M2, M4, M6, and Cf4, grouping different methods. The data correspond to Example 2 with fixed time step size $\tau = 10^{-3}$ for computing $\psi(1)$.

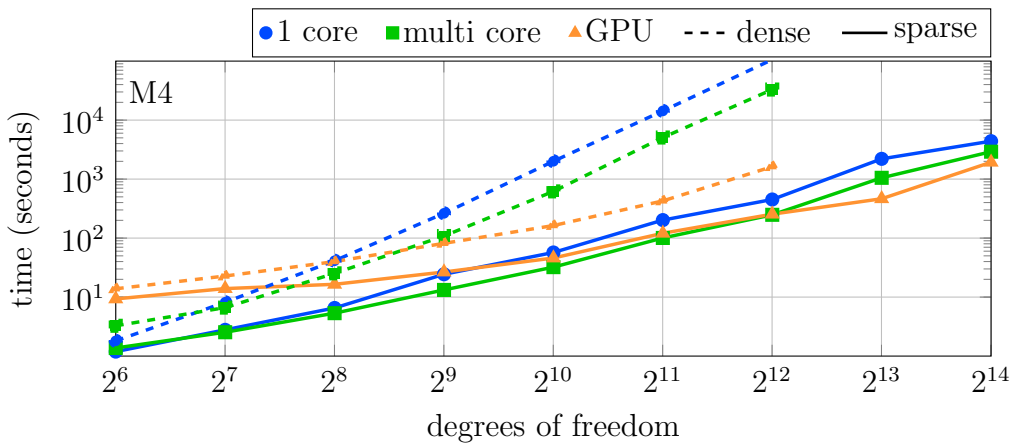


Figure 7: Computational cost vs. degrees of freedom for three different implementations of the integrator M4. The data correspond to Example 2 the solid lines correspond to the sparse implementation and the full lines to the dense representation of the sparse matrix. The time step size is fixed to $\tau = 10^{-3}$ for computing $\psi(1)$. The dense computation stops at 2^{12} due to storage limitations.

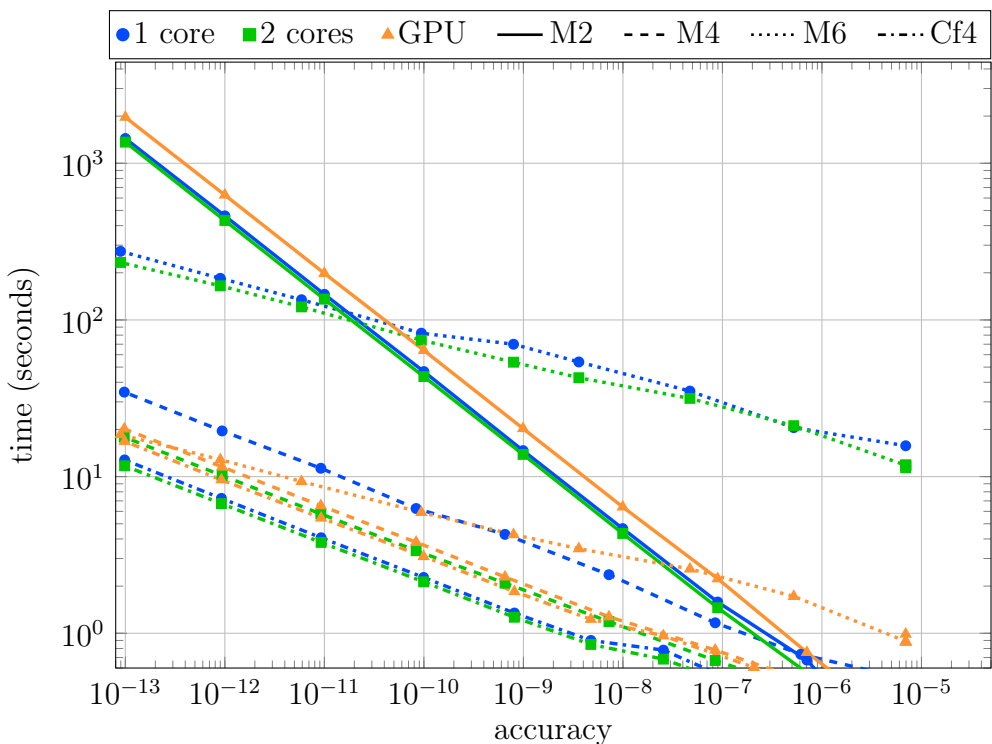


Figure 8: Accuracy vs. computational cost for the four integrators M2, M4, M6, and Cf4 when using different parallelization techniques. The date corresponds to Example 2 with fixed matrix dimension $N = 2^{12}$. For a fixed step size τ the error of $\psi(1)$ is measured.